Bulletin of the Geological Survery of Japan, vol. 53 (2/3), p. 265-283, 2002

2-D and 3-D interpretation of magnetotelluric data in the Bajawa geothermal field, central Flores, Indonesia

Toshihiro UCHIDA[1], Tae Jong LEE[1], Mitsuru HONDA[2], ASHARI[3] and Achmad ANDAN[4]

Toshihiro UCHIDA, Tae Jong LEE, Mitsuru HONDA, ASHARI and Achmad ANDAN (2002) 2-D and 3-D interpretation of magnetotelluric data in the Bajawa geothermal field, central Flores, Indonesia. *Bull. Geol. Surv. Japan,* vol. 53 (2/3), p. 265-283, 15 figs.

Abstract: We conducted MT measurements in the Bajawa geothermal field in central Flores Island, eastern Indonesia, under a joint research project among the Geological Survey of Japan, New Energy and Industrial Technology Development Organization, and Directorate of Mineral Resources Inventory, Indonesia. Then, we have applied two-dimensional (2-D) and three-dimensional (3-D) inversions to the MT data for the geological interpretation of geothermal reservoirs. The inversion algorithms used in this work are based on the linearized least-squares inversion with smoothness regularization. In addition to the subsurface resistivity structure, static shifts in apparent resistivity were also solved simultaneously in the 3-D inversion. The comparison of 2-D and 3-D models has revealed consistent results with each other and that the 3-D inversion technique has become practical. However, there still are some drawbacks in both 2-D and 3-D inversions. When applied to real 3-D environments, the 2-D inversion may create a distorted structure caused by a 3-D structure beneath or off the survey line. On the other hand, since the 3-D technique applied in this work assumes a homogeneous media when computing the Jacobian matrix (sensitivity matrix), it may also create ambiguous anomalies when applied to a structure of large resistivity contrast. The 3-D resistivity models of the major survey area, Mataloko, in Bajawa have the following features. The surface layer is mostly resistive, corresponding to less-altered volcanic rocks, except the geothermal manifestation zone, where resistivity is low from the surface. Below this surface layer is a very conductive layer that spans almost the entire survey area. Beneath the manifestation zone, resistivity is approximately 1 ohm-m and its thickness is approximately 400 - 500 m. This layer is interpreted as the clay-cap of the reservoir system. Pilot drilling data revealed the existence of montmorillonite in this zone. The resistive basement below the low-resistivity layer is interpreted as the hot-water circulation zone. The basement is the shallowest at the manifestation, approximately at a depth of 500 m, while it becomes deeper rapidly in the western half of the surveyed area.

1. Introduction

The electromagnetic (EM) method is one of the most essential tools for investigating geothermal reservoirs. Among various EM methods, the magnetotelluric (MT) and controlled-source audio-frequency magnetotelluric (CSAMT) methods are most commonly applied to geothermal exploration worldwide. The reasons are: 1) these methods can investigate at considerable depths which are suitable for geothermal exploration, 2) productivity and quality of the data have been greatly improved by new field equipment developed in the past decade, and 3) new sophisticated interpretation techniques have been developed and used in many case studies (e.g., Romo *et al.,* 1997; Los Banos, 1997; Bromley *et al.,* 2000; Uchida *et al.,* 2000).

A typical resistivity structure of a geothermal reservoir is characterized by the following two features (e.g., Uchida, 1990; Johnston *et al.,* 1992; Arnason and Flovenz, 1992; Uchida and Mitsuhata, 1995; Uchida, 1995; Arnason *et al.,* 2000; Ussher *et al.,* 2000).

[1] Institute for Geo-Resources and Environment, GSJ
[2] West Japan Engineering Consultants, Inc. Watanabe-dori 2-1-82, Chuo, Fukuoka, 810-0004 Japan
[3] Directorate of Volcanology and Geological Hazard Mitigation, Jl. Diponegoro No.57, Bandung, 40122 Indonesia
[4] Directorate of Mineral Resources Inventory, Jl. Soekarno-Hatta No.444, Bandung, 40254 Indonesia

Keywords: magnetotellurics, 2-D interpretation, 3-D interpretation, resistivity, geothermal reservoir, Bajawa geothermal field, Flores Island, Indonesia

- A reservoir zone generally has lower resistivity than the surrounding non-geothermal areas, because the formation resistivity decreases as the formation temperature increases.
- The lowest resistivity in the reservoir system is usually associated with the cap layer where low-temperature clay minerals, such as montmorillonite, are abundant. On the other hand, the zone of high-temperature hot-water circulation, which is beneath the cap layer, has a higher resistivity than the clay-cap.

These key interpretations have been gradually accepted by geothermal engineers worldwide in the past decade due to the accumulation of high-quality EM case studies by many EM geophysicists.

However, resistivity structures in real geothermal fields are not always simple and vary among geothermal fields. Therefore, more detailed investigations by EM methods at many geothermal fields are necessary for an appropriate interpretation.

In this work, we conducted an MT survey in the Bajawa geothermal field, central Flores, Indonesia in September 1999. It is under the research project called "Exploration of Small-Scale Geothermal Reservoirs in Remote Islands in Eastern Indonesia," which is being jointly conducted by the Geological Survey of Japan (GSJ), New Energy and Industrial Technology Development Organization (NEDO), and Directorate of Mineral Resources Inventory (DMRI). The purpose of the MT survey is to provide integrated information on the electrical resistivity distribution of the Mataloko, Bobo and Nage manifestation areas, in conjunction with the CSAMT data obtained by NEDO and DMRI in 1999 and DC resistivity data obtained by DMRI in 1997 and 1998 (Andan *et al.,* 1997; Uchida and Andan, 1999). We have applied two-dimensional (2-D) and three-dimensional (3-D) inversions to the MT data.

The 2-D inversion is now routinely used for the interpretation of MT and CSAMT data in geothermal exploration and has been successfully providing detailed resistivity information on geothermal reservoirs, because of advanced field equipment and sophisticated 2-D inversion codes that have been developed in the past decade (e.g., deGroot-Hedlin and Constable, 1990; Smith and Booker, 1991; Uchida and Ogawa, 1993; Uchida, 1993; Ogawa and Uchida, 1996; Siripunvaraporn and Egbert, 2000; Rodi and Mackie, 2001).

However, due to complicated geological environments, which we often encounter at geothermal fields, a 2-D interpretation sometimes fails to produce realistic models. The TE-mode data are more sensitive to a deep conductive anomaly in a 2-D situation than the TM-mode data. However, unless the subsurface structure is almost 2-D, we usually can not achieve a good fitting for the TE-mode data in a 2-D inversion. On the other hand, the fitting of the TM-mode data in a 2-D inversion can be more easily achieved even for a 3-D like structure. This is why we often utilize only TM-mode data for 2-D inversion in geothermal exploration. However, even if the data misfit of the TM-mode data is small, the resultant 2-D model may be unrealistic or contain false anomalies. Particularly, the resistivity model of deeper parts of the reservoir structure is often ambiguous. This is also the case for other natural resource exploration and geoscientific researches, such as oil exploration or volcano studies. Therefore, sophisticated 3-D interpretation techniques are now greatly needed for the understanding of true resistivity structures in various applications.

To meet such requirements, there have been intensive researches on 3-D MT inversion in the past decade (e.g., Sasaki, 1999, 2001; Newman and Alumbaugh, 2000; Zhdanov *et al.,* 2000; Sasaki and Uchida, 2001; Hursan and Zhdanov, 2001; Mackie *et al.,* 2001). Since the EM inversion is mostly a nonlinear problem, we usually apply a linearized iterative least-squares scheme in the inversion. For 1-D and 2-D cases, these inversion methods are performed successfully within a relatively short computation time. However, for a 3-D case, a great amount of computation time is required for the linearization in a full 3-D modeling. To overcome this, several approximation approaches have been developed and reasonable resistivity models have been reported (Zhdanov *et al.,* 2000; Mackie *et al.,* 2001). In this work, we use an inversion method that is based on the conventional linearized least-squares scheme (Sasaki, 2001; Sasaki and Uchida, 2001). In this method, the Jacobian matrix (sensitivity matrix) is approximated for a homogeneous media to save the computation time.

We applied the 3-D inversion technique to the MT data obtained in the Bajawa geothermal field in Indonesia. This is one of the first applications of a 3-D interpretation to MT data in geothermal exploration in the world. Our aims are to evaluate how the 3-D program works on real field data and examine the 3-D resistivity features of the geothermal area.

2. MT Data

Flores Island is located in the Nusa Tenggara Timur (NTT) Province, eastern Indonesia. It is one of numerous volcanic islands along the Sunda Island Arc, which spans almost the whole Indonesian country from west to east. The Bajawa geothermal field is located in the central part of the Flores Island (Fig. 1).

Figure 2 is a blown up map of the Bajawa and

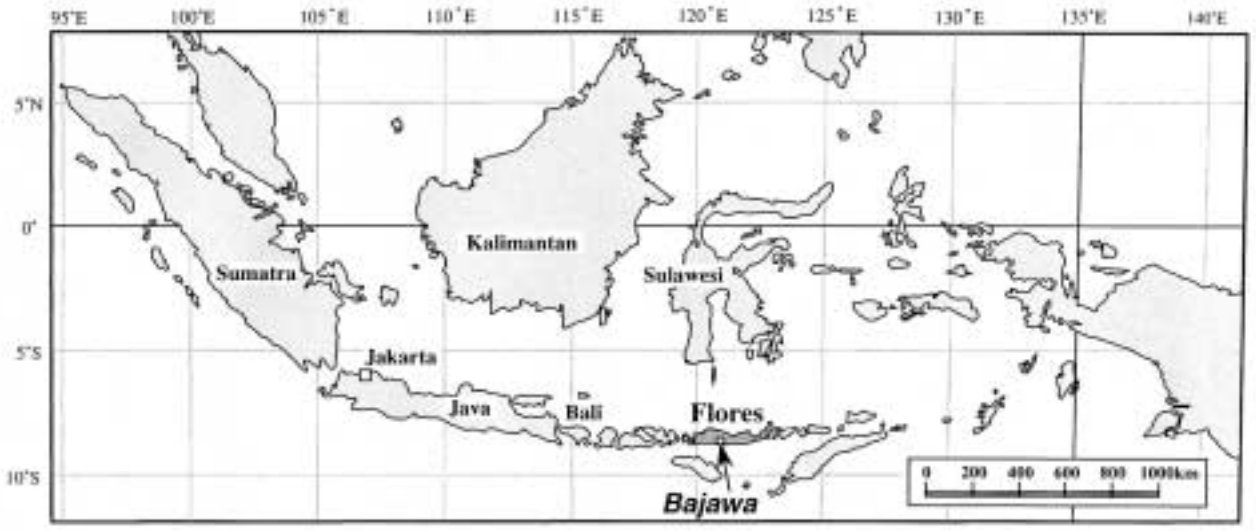

Fig. 1 Location of Flores Island and the Bajawa area.

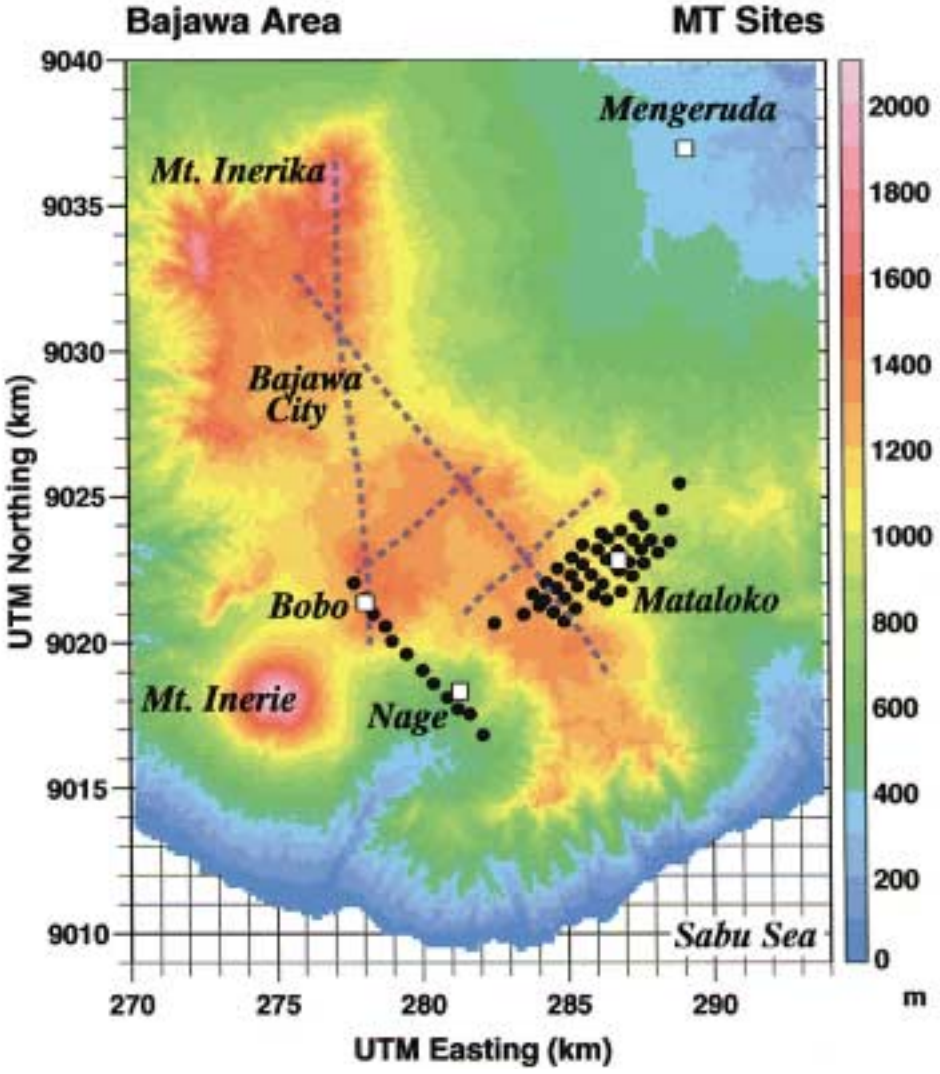

Fig. 2 MT survey stations (black dots) on a topography contour in the Bajawa area. Open squares are major surface manifestations; dashed lines indicate major lineaments of young volcanic cones.

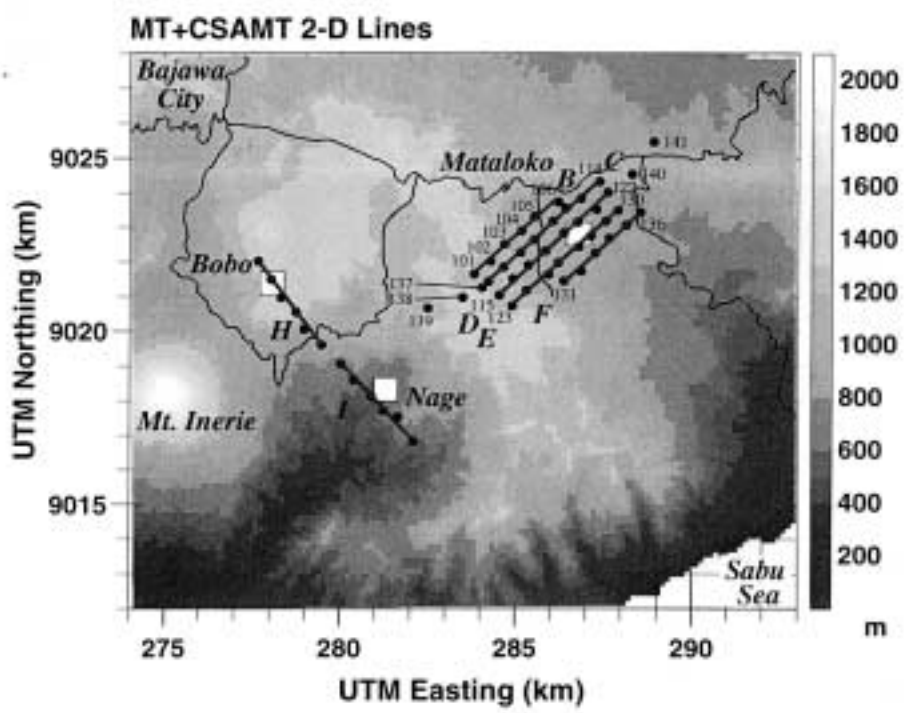

Fig. 3 Survey lines for 2-D interpretation. The CSAMT sites were arranged every 100 m on the survey lines. Station numbers are shown for several MT sites. Thin solid lines are major local roads.

surrounding areas. The survey area is on a highland, whose average elevation is approximately 1000 m. The area is underlain mostly by young volcanic formations (WestJec and MRC, 2000; Muraoka *et al.,* 2000). There are two active volcanoes; Mt. Inerie and Mt. Inerika are west and north of the survey area, respectively. Also, there are numerous small volcanic cones that are younger than 0.5 Ma. Three major surface geothermal manifestations, Mataloko, Bobo and Nage, are located in the studied area. We can recognize a north-south trending lineament of volcanic cones from Mt. Inerika to Bobo. Another trend in the NW-SE direction is seen from the vicinity of Bajawa City to the Mataloko area.

The MT survey lines were arranged to cross the major trend of volcanic cones (Fig. 3). Five NE-SW survey lines, Lines B-F, were arranged around the Mataloko manifestation zone. Two NW-SE survey lines, H and I, were set from the Bobo manifestation to the Nage manifestation zone. The total number of MT stations is 53; 41 on the Mataloko lines and 12 on the Bobo-Nage line. The station interval is approximately 600 m on the lines. The line spacing in the Mataloko area is approximately 500 m. A remote reference site was set up at the Mengeruda manifestation, which is approximately 15 km away north of the Mataloko area (Fig. 2). The MT signal recording was done for 15 hours from evening to the next morning simultaneously at three or four stations, including the remote site. Synchronization between the survey sites and remote site was maintained by a GPS clock signal.

Figure 4 shows examples of MT data at two stations in Mataloko. Figure 4a is an example of good quality data at Station 128 (Line E) and Fig. 4b is an example of poor quality data at Station 111 in a village (Line C). No error bars can be seen in the graphs of apparent resistivity and phase in Fig. 4a, although those with a size of one standard deviation are actually plotted. Small noises at around 60 Hz and 0.1 Hz can be observed at Site 111. The quality of the data is generally very good at most stations as shown in Fig. 4a, not only because there is no large artificial electromagnetic noise sources like power lines, but also the remote reference analysis eliminated local man-made noises or wind noises.

Figure 5 shows distributions of determinant apparent resistivity and induction vectors at four frequencies in the Mataloko area. Apparent resistivity is high at 120 Hz, decreases at 8 Hz and 0.3 Hz, and it becomes large at 0.01 Hz. The contours at 8 and 0.3 Hz show a large low resistivity anomaly located at the center of the survey area, which is near the manifestation zone. The total conductance of the low-resistivity layer must be large in this zone.

The tipper amplitude is small at high frequencies above 1 Hz; then increases as the frequency decreases (Fig. 4). The induction vector points toward a zone whose resistivity is smaller than the station. When the tipper is small (the induction vector is short), lateral change of resistivity is small. On the

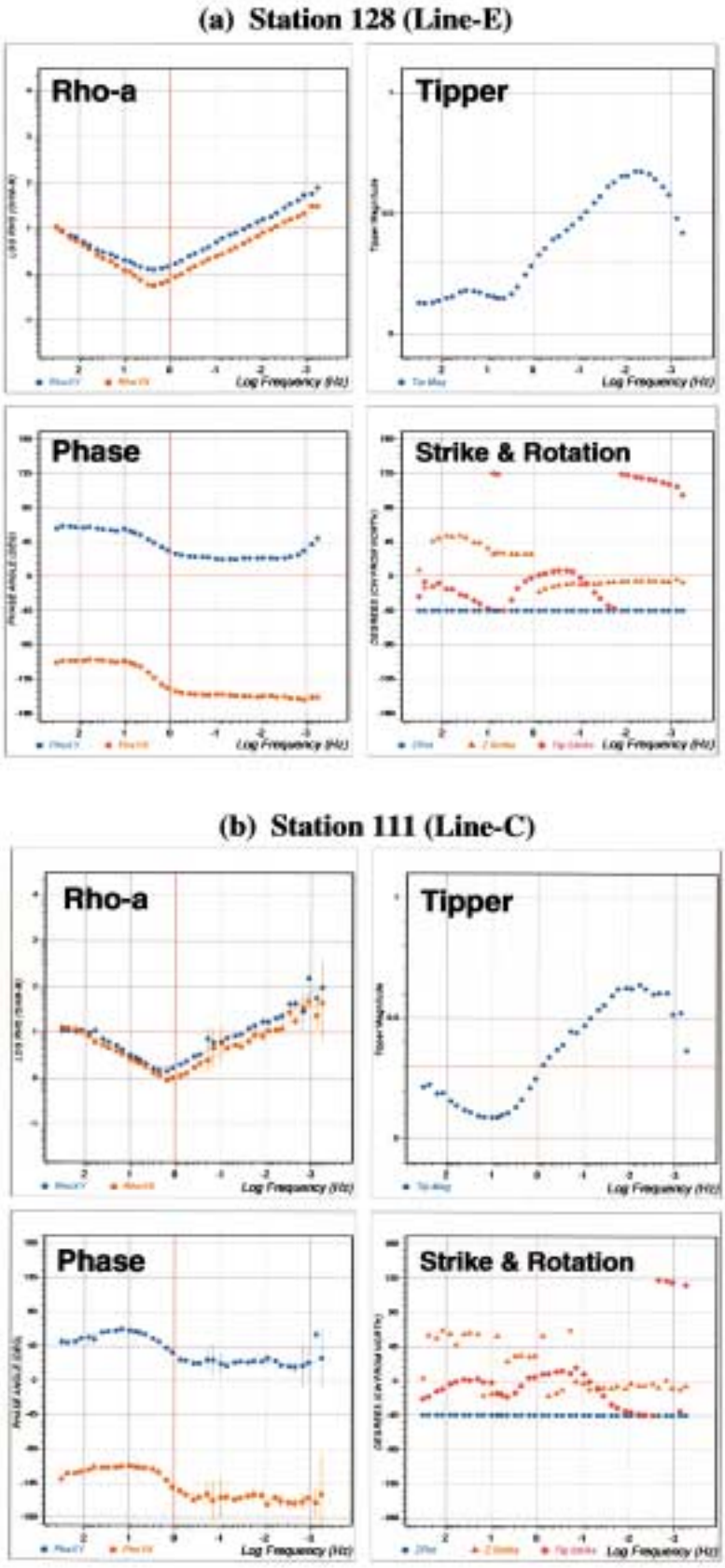

Fig. 4 Examples of MT data in the Mataloko area: (a) Station 128 on Line E, and (b) Station 111 on Line C. Apparent resistivity (upper-left), phase (lower-left), tipper magnitude (upper-right), and strikes and rotation direction (lower-right) are shown. The impedance is rotated to the direction of -45 degrees (northwest). Error bars of one standard deviation are also shown.

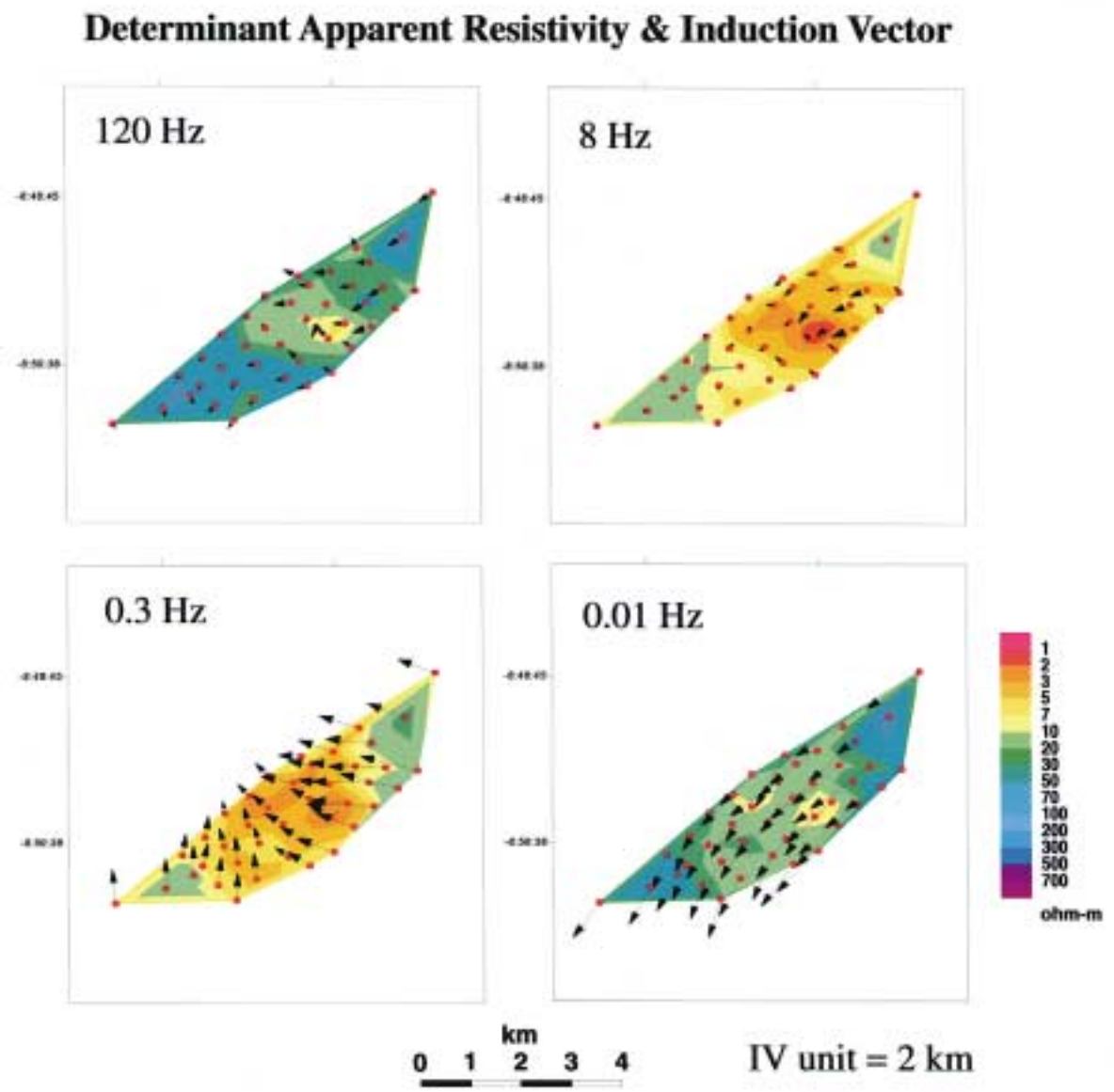

Fig. 5 Distribution of determinant apparent resistivities and induction vectors in the Mataloko area at 120 Hz (upper-left), 8 Hz (upper-right), 0.3 Hz (lower-left) and 0.01 Hz (lower-right). The unit of the induction vector corresponds to the length of 2 km.

other hand, if the tipper is large, the station is located on a zone of rapid resistivity change in the lateral direction. For example, the vectors generally point northwestward at 0.3 Hz. It means that a large low-resistivity zone is located in the northwestern part of the survey area. A typical depth of such a low-resistivity layer is approximately 2 km, which is the skin depth when we assume a resistivity of 5 ohm-m at 0.3 Hz. At 0.01 Hz, all the induction vectors are large and point southward, because there is a huge low resistivity zone far to the south, which is the Indian Ocean (Sabu Sea).

3. 2-D Interpretation

3.1 Inversion Procedure

We carried out a 2-D inversion for all survey lines in the Mataloko and Bobo-Nage areas. Since CSAMT data were obtained by NEDO and DMRI at the same time, we also incorporated them into the inversion (Fig. 3).

We rotated the MT impedance to the direction of the survey line, assuming that the strike direction is perpendicular to the line. We used so-called TM mode data, which is an electric field in the line direction and a perpendicular magnetic field, for the inversion. The number of frequencies used was 12, ranging from 0.07 Hz to 120 Hz.

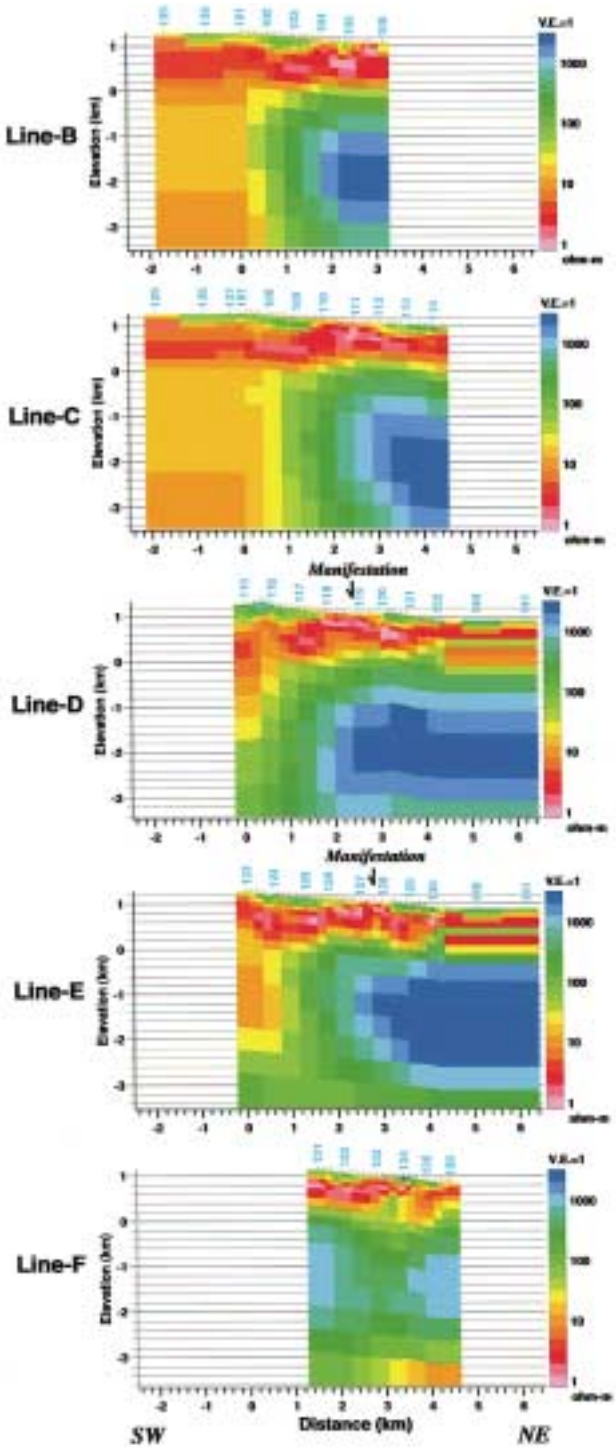

Fig. 6 The 2-D models of the survey lines in the Mataloko area. Both MT (TM mode) and CSAMT data were used for the inversion. Site numbers are shown only for MT stations.

The interval of CSAMT and MT sites was 100 m and approximately 600 m, respectively. At a site where both CSAMT and MT data were obtained, the MT apparent resistivities were shifted to fit the CSAMT apparent resistivities. The number of CSAMT frequencies used was 8, ranging from 8 Hz to 1024 Hz. The CSAMT phases at high frequencies were somewhat biased, so they were removed from the observed data.

Both apparent resistivity and phase were used as the observed data. Minimum noise assumed was 3 % in the apparent resistivity and an equivalent amount in the phase for MT data. A 5 % noise was assumed for all CSAMT data, because no information on observation errors was available. The forward modeling was done by the finite-element method with topography incorporated. The inversion method that was used is the linearized least-squares scheme with smoothness regularization. The minimization of the data misfit and model roughness is simultaneously achieved by introducing the Bayesian likelihood (Uchida and Ogawa, 1993; Uchida, 1993).

3.2 Mataloko Lines

Figure 6 shows the resistivity models obtained by 2-D inversion of the five survey lines in the Mataloko area. Notice that the same two sites, 138 and 139, were used on the left end of Lines B and C. Sites 140 and 141 were used for the right end of Lines D and E. Figure 7 compares the observed and modeled MT responses of all sites on Line E.

The inversion was stably performed. Although the final root-mean-squares (rms) misfit is still 1.7 for Line E, the fitting between the observed and theoretical apparent resistivities and phases is very good (Fig. 7). The detailed shallow structure, shallower than 1 km, was determined very well due to the dense CSAMT sites.

The typical features of the 2-D models are as follows:

- There is a thin surface layer of high resistivity, except the zone around the Mataloko manifestation. It corresponds to volcanic rocks and tuffs that have experienced only a little alteration.
- Below this surface layer is a very low-resistivity layer. It is distributed almost over the entire survey area. An average thickness at the center of the area is several hundreds of meters, and resistivity is very low, as low as 1 ohm-m. Although the surface manifestation is observed only around Lines D and E, the area of this low resistivity layer is much wider. The low resistivity layer becomes thicker in the western part of the area, but resistivity also becomes higher.
- There is a high resistivity layer in a deeper zone. The average elevation at the center zone is slightly above the sea level. Resistivity of the

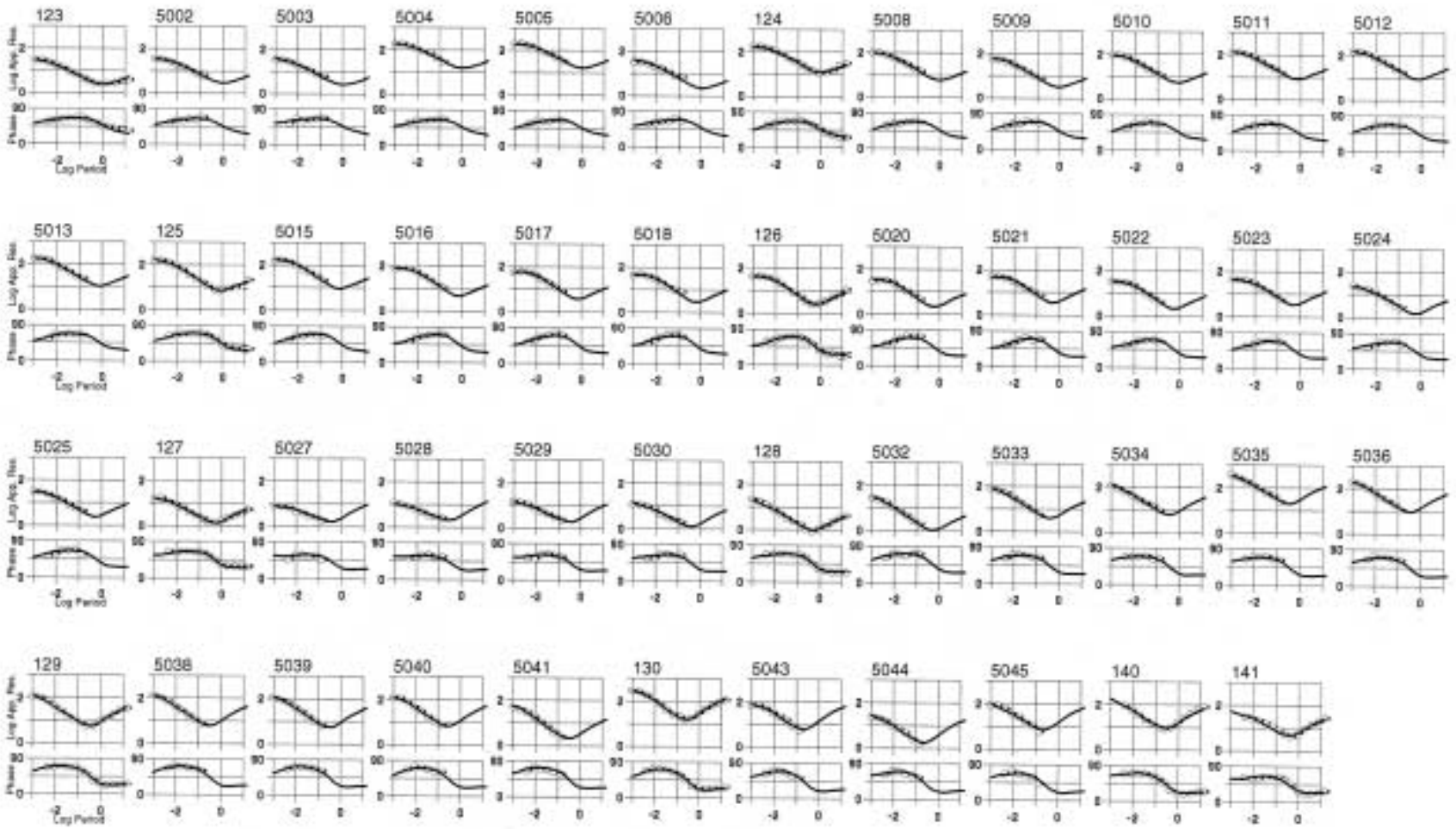

Fig. 7 Comparison of observed and modeled MT responses at all sites on Line E. Open circles are observed data and the lines are theoretical ones obtained from the model shown in Fig. 6. Site numbers for CSAMT-only stations are in four digits.

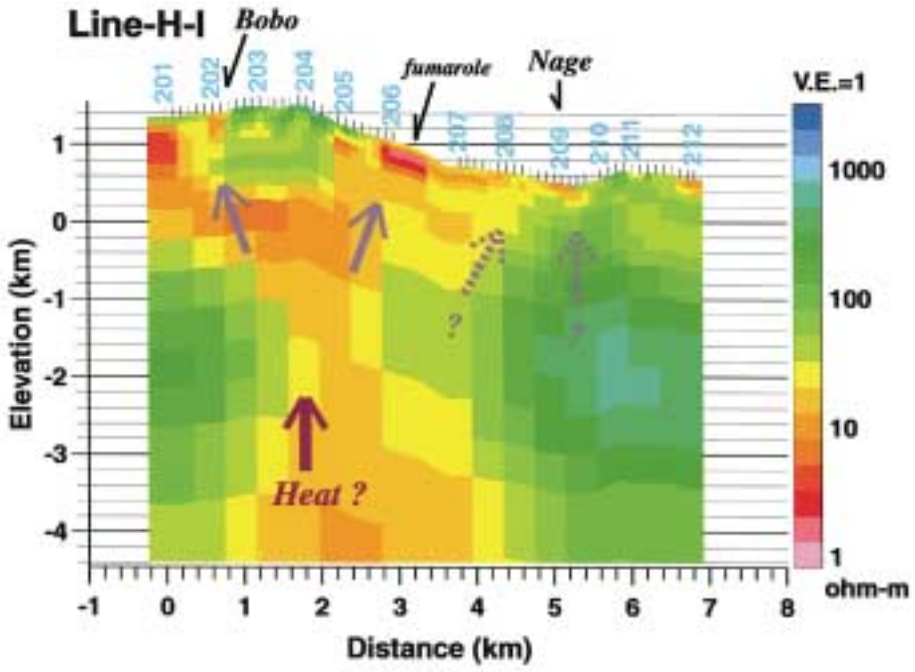

Fig. 8 The 2-D model of the survey lines in the Bobo-Nage area. Preliminary geothermal interpretations are also shown.

layer is generally higher at the eastern side of the area, where a maximum resistivity of more than 1000 ohm-m was interpreted.

These models are consistent with 2-D models obtained by the inversion of Schlumberger data obtained in 1997 and 1998 (Uchida *et al.,* 2002). A detailed interpretation of the Mataloko MT data will be discussed in the section of 3-D interpretation later.

3.3 Bobo-Nage Line

Figure 8 shows the 2-D inverted model of the Nage-Bobo line. The data of both Line H (west half) and Line I (east half) were inverted simultaneously. Line H crosses the Bobo manifestation that is located on a slope of a volcanic cone. Line I does not directly cross the Nage manifestation zone that is located in a basin structure (Fig. 3), but passes the southern edge of the Nage manifestation. Since the topography is very steep in the Bobo and Nage areas, the quality of the MT data at some sites and phase data at many CSAMT sites was poorer than the Mataloko data.

The resistivity structure of the Bobo-Nage line is more complicated than the Mataloko area. The shallow part of the Bobo area is characterized by a resistive body that corresponds to young volcanic cones. A shallow low-resistivity anomaly can be recognized at the Bobo manifestation corresponding to the alteration zone in the manifestation. Below the resistive body, there is a large low-resistivity layer at around the sea level. It continues westward then upward to the Bobo manifestation. On the eastern side, it outcrops around sites 206 and 207, where another surface alteration zone and fumarole are recognized at the surface. The low-resistivity layer at the sea level might be associated with a high-temperature zone of the Bobo volcanics.

On Line I, there is a shallow low resistivity anomaly at Nage. However, its size is small and its resistivity, around 10 ohm-m, is not so low compared with the Mataloko manifestation. Also, there is a large high-resistivity zone below sea level.

There are a large surface alteration zone and outflows of hot water and steam in the Nage area. The geological survey indicates that the volcanic rocks in the Nage area is older than 1 Ma and form a basement of the young post-caldera volcanics (WestJec and MRC, 2000). The high-resistivity body in the deeper portion may correspond to the old volcanic rocks that have not experienced intensive alteration. However, the resistivity model can not tell the location of the upflow path where the deep geothermal water moves to the surface.

One interpretation is that hydrothermal water flows from the roots of the Bobo volcanoes, probably below sea level, to Nage as indicated by the large low resistivity layer that continues from the deeper part of Bobo to Nage. Another interpretation is that the geothermal system beneath Nage does not produce much low-temperature clay minerals, such as montmorillonite, and the formation resistivity does not become low, even though there are fluid paths in the basement from directly beneath the Nage area.

4. 3-D Interpretation

4.1 Inversion Scheme

The 3-D inversion scheme used in this work is based on the linearized iterative least-squares method with smoothness regularization (Sasaki, 1999, 2001). The forward modeling for a given arbitrary 3-D earth was by the finite difference method (FDM). The electric field was first solved in frequency domain. Then, the magnetic field was computed from the obtained electric field. For a finite difference with a staggered grid, the solution region, including both air and earth, was discretized into rectangular cells. The topography was not incorporated.

The Jacobian matrix consisting of partial derivatives (sensitivities) of MT responses with respect to block resistivities in the 3-D model should be evaluated from an estimated model at each iteration in the usual iterative least-squares inversion. However, in this work, sensitivities of the MT responses were once obtained for a homogeneous earth, and the same sensitivities were used at all iteration steps.

In addition to block resistivities in a 3-D model, static shifts were also treated as unknowns in the inversion (Sasaki, 2001). A static shift is caused by shallow small inhomogeneities, and observed as a frequency-independent bias on apparent resistivity values, without changes in phase values. The amount of the shift is completely arbitrary and impossible to estimate from the observed apparent resistivity data. In our inversion, a Gaussian distribution of static shifts was assumed. We applied a regularization that the norm of static shifts is close to zero.

To stabilize the model correction at each iteration step, smoothness regularization was adopted. An optimum smoothness was searched based on the misfit minimization at each iteration. However, optimization of the weight for the static-shift minimization was basically by a trial-and-error basis.

The objective function U to be minimized in the inversion is defined as

$$U=\|W[d-F(m)-Gs]\|^2+\lambda^2\left(\|Cm\|^2+\beta^2\|s\|^2\right) \quad (1)$$

where W is the weight defined from observation errors, d is the observed data (apparent resistivity and phase), m is a 3-D resistivity model, F is a nonlinear function that works on the model m to produce MT responses, C is a roughening matrix, s is static shifts, and G is a matrix that relates static shifts and the MT responses. The first term of the right-hand side is for the misfit minimization and second term is for roughness and static-shift minimization. The λ and β are trade-off parameters for roughness minimization and static-shift minimization, respectively, with regard to the misfit minimization.

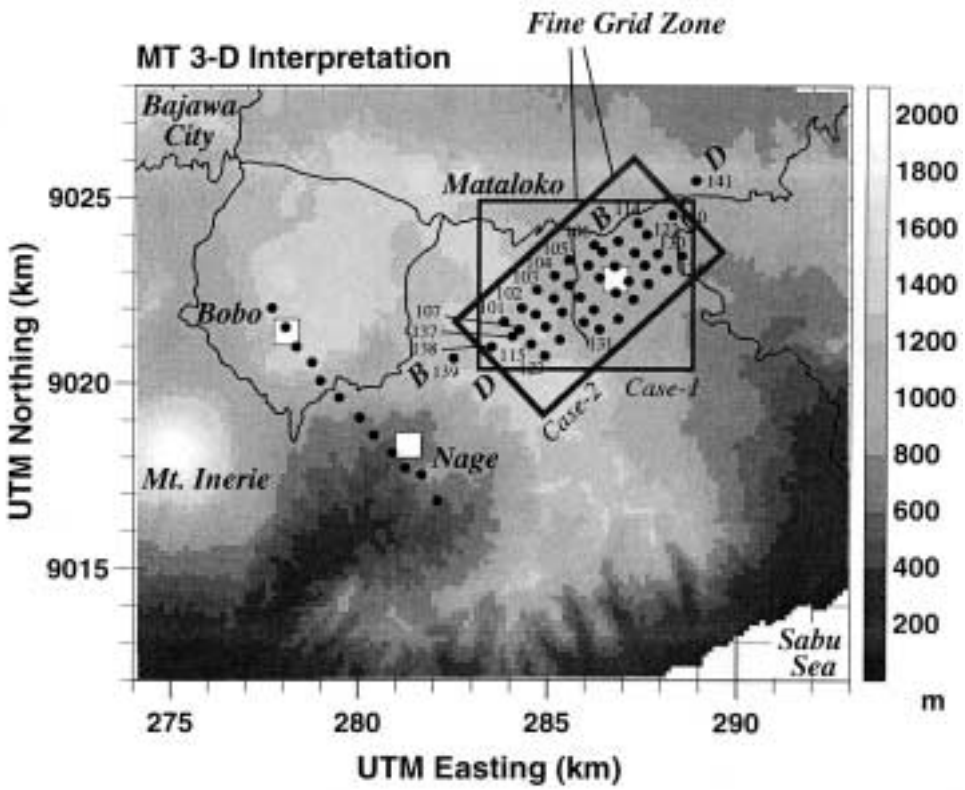

Fig. 9 Two mesh settings, Case-1 and Case-2, for 3-D interpretation in the Mataloko area. Rectangles indicate the zones of fine grid for the finite-difference mesh discretization.

We applied the 3-D inversion to the MT data at the Mataloko area (Fig. 9). There were 39 MT sites used for the 3-D inversion. Since the 3-D inversion code currently utilizes only the off-diagonal components of the impedance, Z_{xy} and Z_{yx}, it may be important to choose an appropriate rotation direction. Therefore, we selected two rotation directions: 90 degrees (x-axis is east) and 45 degrees (x-axis is northeast). We refer to the former case as Case-1 and the latter as Case-2. Then, we carried out 3-D inversion for each dataset with different mesh discretization (Fig. 9) in order to compare the effect of the rotation direction in the final models.

Twelve frequencies, from 0.03 Hz to 60 Hz, were used for the inversion. The size of the cells at the surface in the interpreted zone (shown by rectangles in Fig. 9) was 200 m (or 125 m) horizontally and 100 m vertically. Gradually coarser cells were added outside the interpreted zone. The number of finite difference cells was approximately 50 - 60 in the x- and y- directions and 33 in the z-direction. In the inversion code, MT stations must be at the surface nodes of the finite difference mesh. Therefore, the location of each MT station was shifted to the nearest node point on the mesh.

The initial model was a homogeneous half space, whose resistivity was the average of the observed apparent resistivities. The partial derivatives were obtained from the initial model. The underground resistivity structure was represented by numerous rectangle blocks whose resistivities were dealt unknown in the inversion. The size of the blocks is approximately 400 m horizontally. The numbers of observed data was 1870, and the number of model parameters was 1900 for Case-1 and 1820 for Case-2. The MT responses used for the inversion were apparent resistivities in natural logarithmic domain and phases. For the weighting matrix W, a noise floor of 1 % was assumed.

Selection of the optimum smoothness was done based on the misfit minimization. Among several candidate values of λ, the value that provided the smallest misfit was chosen at each iteration. Regarding the trade-off for the static shift minimization, we tried a few values of β and compared the final misfits.

Figure 10 shows how the rms misfit decreased as a function of iteration with respect to parameter β for Case-1. When β is large, the solved static shifts are relatively small. On the other hand, when β is small, the bias of apparent resistivity curves tends to be explained mostly by static shifts. We can recognize that if we do not include static shifts as unknowns, the rms misfit can not become small after a certain number of iterations. If β is too small (e.g., $\beta=1$), the rms misfit does not decrease much after several iterations. When β is 2 or 4, the misfit continues to decrease. Although the final rms misfit of approximately 8 is still a large value, we decided to use the model using $\beta=2$ in this case.

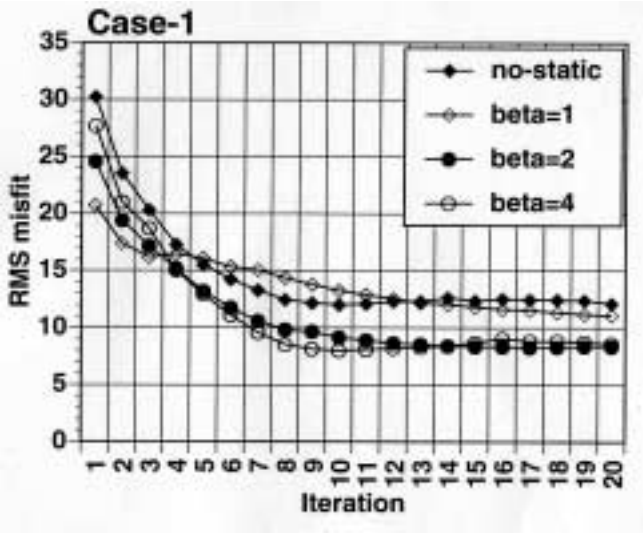

Fig. 10 The rms misfit as a function of iteration numbers in the 3-D inversion for Case-1. Four values of β were tested for the trade-off between the minimization of the data misfit and norm of static shifts.

4.2 Inversion Results

The 3-D models obtained by the inversion for Case-1 and Case-2 are shown in Figs. 11 and 12 as depth-slice sections. Figure 13 shows examples of MT responses on Line E.

When there is a gap between apparent resistivities of the two components, Z_{xy} and Z_{yx}, at high frequencies and we do not consider static shifts in the inversion, high frequency apparent resistivities can not be explained by a 3-D model (see Site 124 in Fig. 13a). However, these gaps can be well matched by assuming appropriate static shifts (Fig. 13c). In the latter, the pure 3-D responses mostly try to fit to the phases and the shape of apparent resistivity curves (Fig. 13b). This means that the consideration of the static shift is necessary for the 3-D inversion unless we use very small blocks for shallow layers.

Although the data look different between the two rotation directions, Case-1 and Case-2, both data were well explained by individual inversions (Figs. 13c and 13d). Also, the two models obtained by inversions for Case-1 and Case-2 are very consistent with each other in the interpreted zone (Figs. 11 and 12), showing the same resistivity patterns in details on each depth slice. The average of the estimated static shifts is approximately 0.3 in natural logarithm for both cases. These results indicate that the rotation direction is not so crucial for a 3-D inversion even though we only used the off-diagonal components of the impedance.

In the 3-D discretization, we moved the location of the MT stations to the nearest node points on the

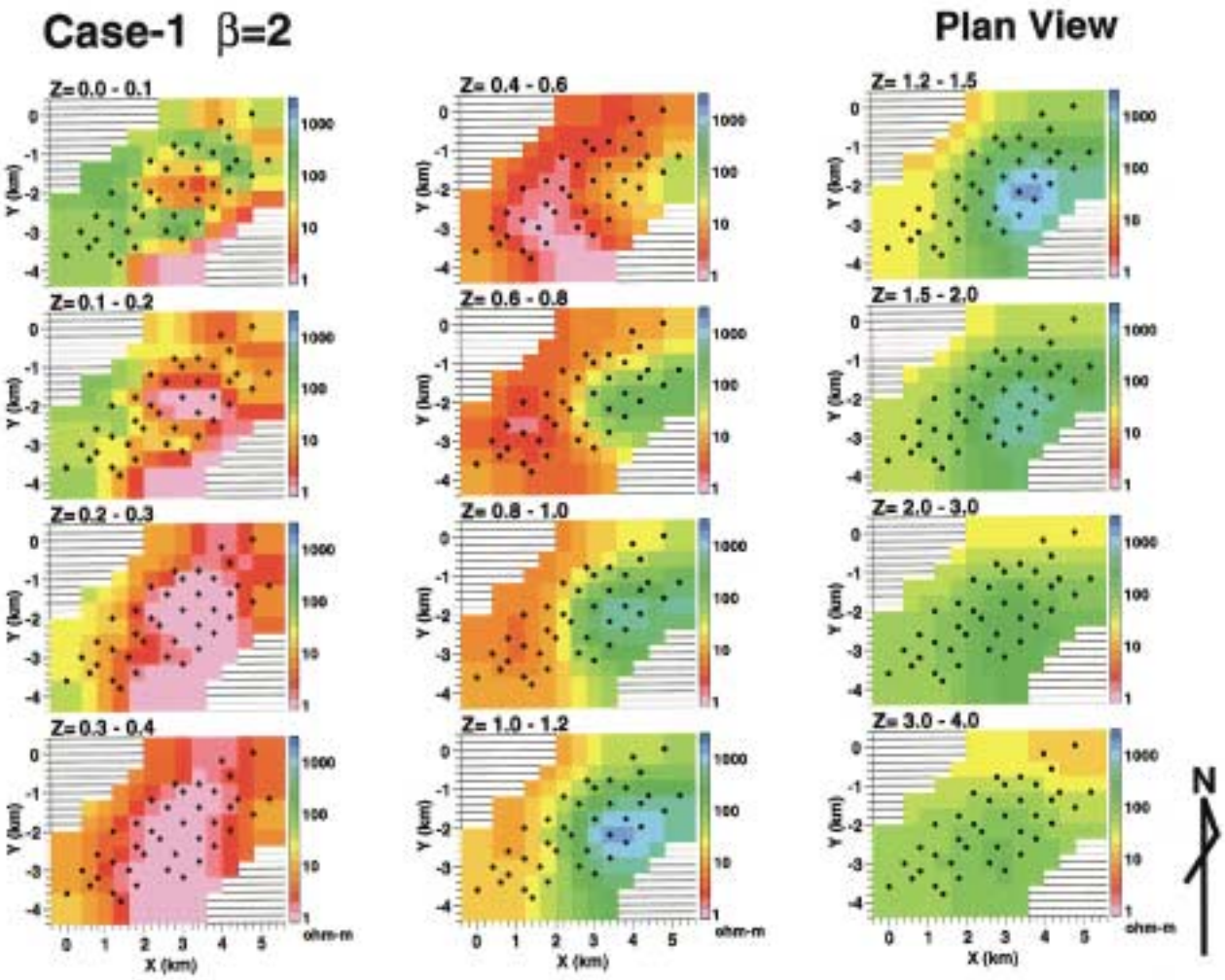

Fig. 11 The 3-D depth slice model of the inversion for Case-1. The trade-off parameter for static shift, β, is 2. Small black dots indicate MT stations.

3-D mesh by a maximum of 100 m. These movements are almost random and different between Case-1 and Case-2. Judging from the similarity of the two 3-D models, it seems that the effect of these movements is not significant.

When we compare the apparent resistivities of the Case-1 and Case-2, the splitting between the two components, Z_{xy} and Z_{yx}, at lower frequencies is bigger for Case-1 than Case-2 (Fig. 13). It indicates that the major strike direction in the deep structure is either N-S or E-W. It is consistent with the shape of the high resistivity anomaly detected by the two 3-D models in Figs. 11 and 12.

When we check the impedance skew in the original data, the skew values are generally small, less than 0.3, at many stations. It means that three-dimensionality is not so significant in this field. However, there are observed high skew values, greater than 0.3, at low frequency data at several stations in the northeastern part of the surveyed area. The reason is that the deep high-resistivity basement has a 3-D shape and creates a significant three-dimensionality.

The western half of the deep model is characterized by a low-resistivity zone from a depth of 400 m to 1.5 km. When we assume an average resistivity of 1 - 2 ohm-m, this is consistent with the induction vectors at 0.3 Hz that point west or northwest directions (Fig. 5), suggesting that the low resistivity body expands to this direction outside of the surveyed area.

Figure 14 compares the 3-D models with 2-D inversion models on survey lines B and E. Note that the 2-D models utilize the dense CSAMT data as well as the MT data. The horizontal size of the surface blocks is 100 m for the 2-D models and 400 m for the 3-D models. Therefore, the 2-D models can provide a more detailed structure for shallow parts, while resistivity distribution in the 3-D models is smooth. Even so, the general features of these sections agree very well.

The shapes of the high-resistivity surface layers are almost the same. Lower boundaries of the low-resistivity layers are also almost the same between

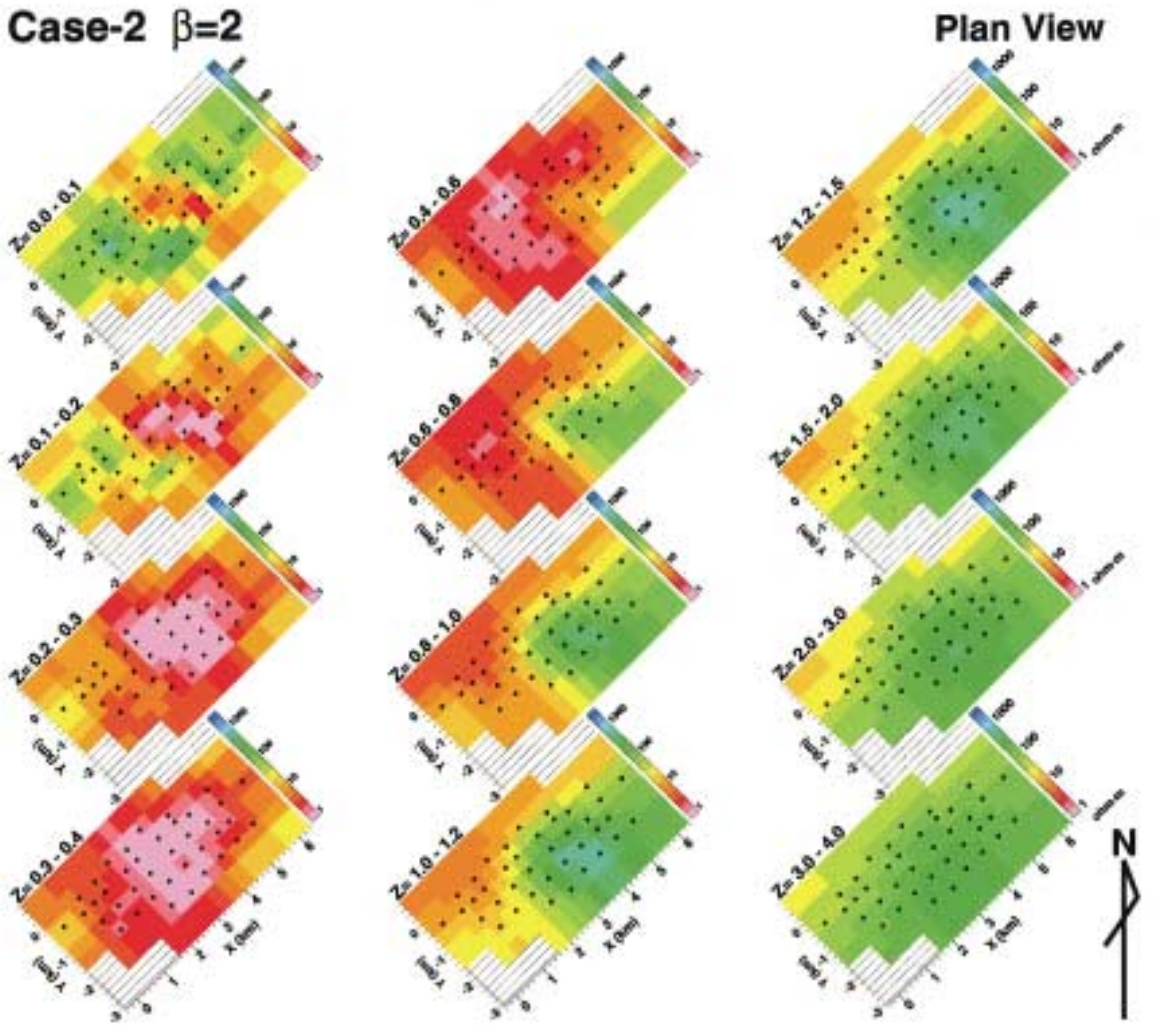

Fig. 12 The 3-D depth slice model of the inversion for Case-2. The trade-off parameter for static shift, β, is 2. Small black dots indicate MT stations.

2-D and 3-D. Very conductive anomalies in this layer, around 1 ohm-m, are more scattered in the 2-D models, but are more concentrated beneath the center of the lines in the 3-D models.

Resistivity distribution in the resistive basement is different between the 2-D and 3-D models. Very resistive zones were obtained by 2-D inversions on the right side of the sections for both Lines B and E. The difference is more significant for Line B. When we only use TM-mode data for 2-D inversion, resolution for deep structures usually becomes poor. We recognized from the 3-D models that the major strike of the resistive basement is in the east-west direction. However, the 2-D lines are oriented in the NE-SW direction. Therefore, the deep resistive anomaly in the 2-D model of Line B may be an artifact caused by a lateral effect from this 3-D-shaped resistive basement east of Line B.

On the contrary, we should also note that these 3-D models contain ambiguities because the Jacobian matrix is based on the assumption of a homogeneous media. The deep resistive anomaly in the eastern half of the 3-D model may not be accurately inverted, because the Jacobian matrix for these blocks is inaccurate due to the very low-resistivity layer located above them.

Although the quality of the observed data was very good, the final rms misfit, normalized by the 1 % noise-floor weight, is approximately 8 for Case-1 and 7 for Case-2. This means that the 3-D models are not able to explain the observed data perfectly. If it is a 2-D case of the TM mode, the inversion can reduce the misfit more but produces some artifacts or extreme structures. However, for a 3-D case, it is difficult to explain both the Z_{xy} and Z_{yx} data simultaneously. Therefore, we can not help staying on a smoother model. It may be a limitation of the current 3-D technique and should be a research subject in the near future.

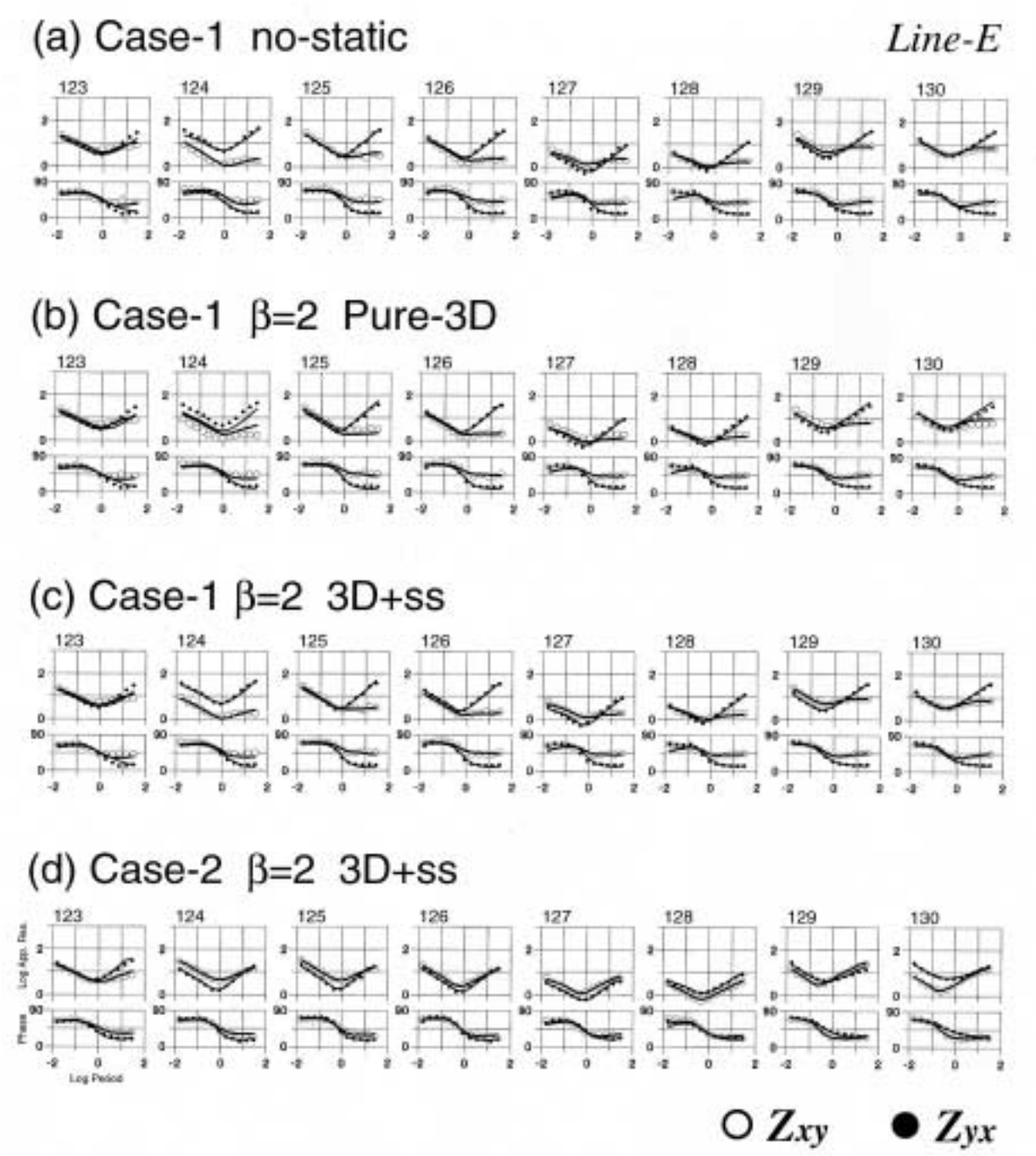

Fig. 13 Examples of 3-D responses on Line E in Mataloko. Circles are observed data, and lines are computed data. Open circles are the xy-components and solid circles are yx-components. (a) 3D responses for Case-1 without static shift consideration, (b) pure 3D responses for Case-1 with $\beta=2$, (c) 3D responses and static shifts combined for Case-1 with $\beta=2$, and (d) 3D responses and static shifts combined for Case-2 with $\beta=2$.

5. Geological Interpretation

Figure 15 shows a preliminary geological and geothermal interpretation of the 3-D MT models. A surface alteration zone was recognized at the center of the Mataloko area by a geological survey (Fig. 15, upper-right figure). The size of the alteration zone is relatively small on the surface; approximately 1 km in length along a small creek in the east-west direction. A geochemical survey revealed a high mercury concentration in the same zone, which is widely extending in the NE-SW direction (WestJec and MRC, 2000). The surface low resistivity anomaly, which is extending in the east-west direction, is much wider than these two geological and geochemical anomalies (Fig. 15, upper-right figure). There seems to be a shallow hidden (does not outcrop) alteration zone that is surrounding the surface alteration zone and much wider than

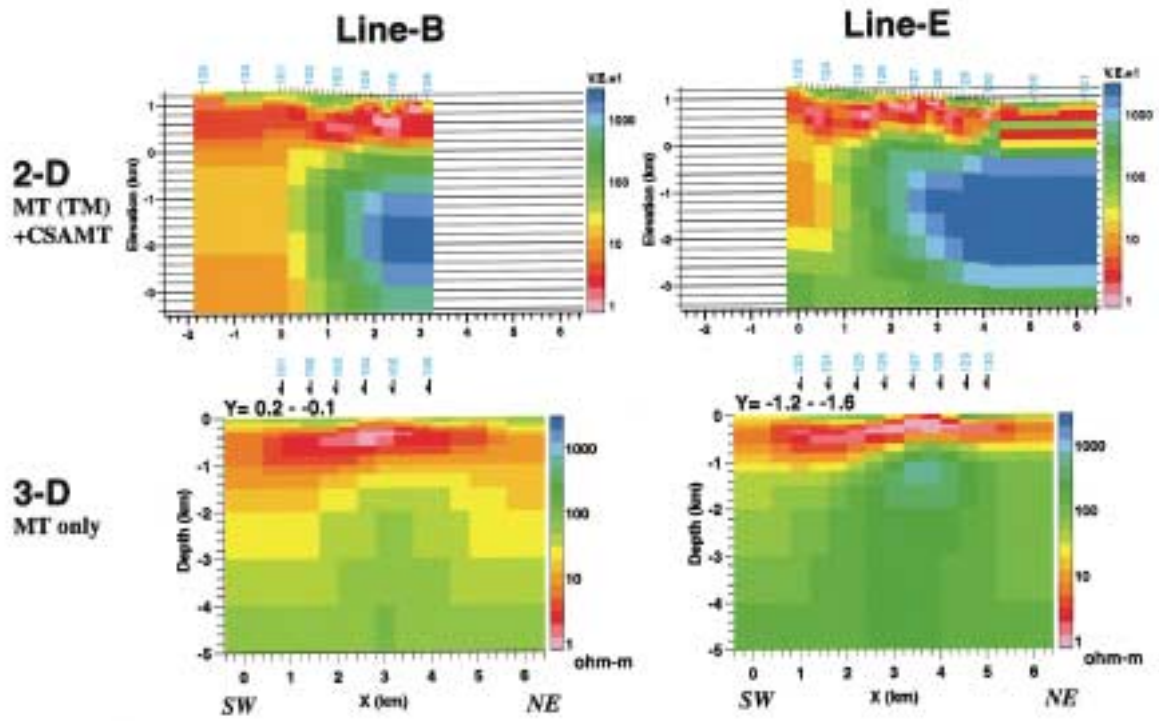

Fig. 14 Comparison of 2-D and 3-D models on Lines B and E in Mataloko. The 3-D sections are extracted from models in Fig. 12.

the anomalies. The hidden alteration zone must be overlain by a very thin high-resistivity layer, because even the highest frequency (120 Hz) data did not detect it but directly responded to the low-resistivity hidden alteration zone.

The low-resistivity layer at depths between 100 m and 500 m widely spreads in the Mataloko area. Particularly, the very conductive zone, around 1 ohm-m, has a size of greater than 2 km in the east-west direction at a depth of 250 m (Fig. 15, middle-right figure).

The NEDO drilled two shallow exploration wells, MT-1 and MT-2, with a total depth of 207 m and 162 m, respectively, near the manifestation in Mataloko in the year 2000 (WestJec and MRC, 2001). From the analysis of the cuttings, they recognized kaolinite and montmorillonite in volcanic rocks as major clay alteration minerals. The very conductive layer corresponds to the montmorillonite-rich zone, and it can be interpreted as the cap layer of the reservoir system. They also recognized wairakite from the bottom of the wells. It indicates that high-temperature hot water circulated up to this depth level. However, thickness of the low-resistivity layer is more than 400 m near the drilling sites, and the thickness of the clay cap must also be a similar value. Therefore, the high-temperature hot water seems to have circulated upward through permeable fractures in the cap layer.

A deep high resistivity anomaly can be seen in the eastern half of the 3-D model. The shallowest portion is beneath or east of the manifestation. This can be interpreted as the reservoir zone of the geothermal system. Of course, it is not possible from the existing survey data to identify the locations of the upflow zone of the geothermal circulation and the heat source of the geothermal system. Also, it is not easy to identify any fault structures or discontinuities in the high resistivity anomaly, other than the discontinuity that is surrounding this high-resistivity anomaly. However, we can say that this portion is a potential target of future development.

6. Conclusions

We conducted an MT survey in the Bajawa geothermal field in central Flores Island, eastern Indonesia, under a joint research project among DMRI, NEDO and GSJ on the exploration of small-scale geothermal resources of the remote islands in Indonesia. We have applied 2-D and 3-D inversions to the MT data for the geological interpretation of geothermal reservoirs.

The 3-D inversion algorithm used in this work is based on the linearized least-squares inversion with smoothness regularization. In addition to the subsurface resistivity structure, the static shift in apparent resistivity was also solved simultaneously in the inversion.

The following were understood through the 3-D inversion.

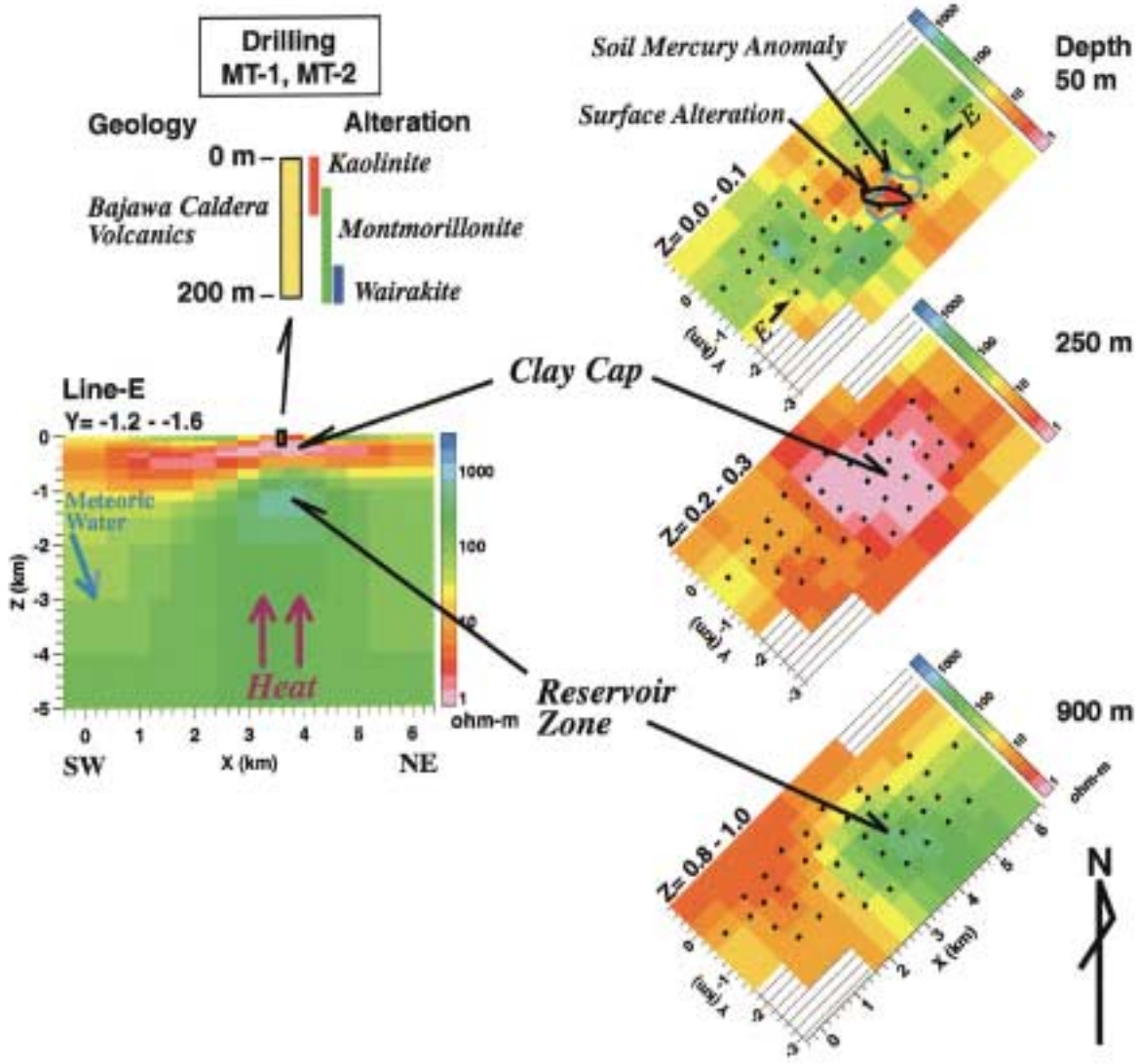

Fig. 15 Interpretation of 3-D resistivity models for geothermal reservoirs in the Mataloko area. Zones of surface alteration and soil mercury anomalies greater than 2.4 ng/cm^3 are shown in the upper-right figure (WestJec and MRC, 2000). Drilling data for wells MT-1 and MT-2 are also shown in the upper-left figure (WestJec and MRC, 2001).

- Although we used the Jacobian matrix of a homogeneous half space for all the iteration steps, the inversion worked well for real field data.
- Inclusion of the static shift in the inversion is essential to achieve a sufficient fitting for high-frequency apparent resistivities.
- Rotation direction of the MT impedance and direction of the mesh discretization are not crucial for the final results.

Comparison of the 2-D and 3-D models has revealed that the results are consistent with each other and the 3-D inversion technique has become practical. However, there still are some drawbacks in both 2-D and 3-D inversions. When applied to real 3-D environments, 2-D inversion may create a distorted structure caused by a 3-D structure beneath or off the survey line. The deep resistive anomaly obtained in the 2-D model of Line B may be an artifact caused by a lateral effect from the 3-D-shaped resistive basement located east of Line B. On the other hand, since the 3-D technique applied in this work assumes a homogeneous media when computing the Jacobian matrix, it also may create ambiguous anomalies when applied to a structure of large resistivity contrasts.

The 3-D resistivity models of the Mataloko area are characterized by the following features:

- Surface layer is mostly resistive, corresponding to less-altered volcanic rocks, except the manifestation zone, where resistivity is low from the surface. This low-resistivity zone is wider than the area of surface alteration and soil mercury anomaly.

- Below this resistive layer is a very conductive layer that spans almost the entire survey area. The resistivity is very low, as low as 1 ohm-m, beneath the manifestation zone. Its thickness is approximately 400 - 500 m at the manifestation zone. This layer is interpreted as the clay-cap of the reservoir system. Pilot drilling data revealed the existence of montmorillonite in this zone.
- The resistive basement, below the low-resistivity layer, is the shallowest, at approximately a depth of 500 m, beneath the manifestation. It rapidly becomes deeper in the western half of the surveyed area. This layer corresponds to the hot-water circulation zone of the reservoir system, and can be a target of future development.

The 2-D resistivity model of the Bobo and Nage areas are as follows:

- Two manifestation zones, Bobo and Nage, are characterized by small shallow conductive anomalies.
- The bodies of the Bobo volcanic cones are resistive. However, there is a deep conductive layer around sea level. It may be associated with a high-temperature zone of the volcano system.
- The path of hydrothermal water upflow to the Nage manifestation is not interpreted clearly from the resistivity model. It may be either from the deep heat source beneath the Bobo volcanic cones or from an unknown source directly beneath the Nage area.

It is obvious that 2-D interpretation has limitations when applied to complicated 3-D environments in geothermal fields. The 3-D inversion has been applied to MT field data for geothermal exploration in this work for the first time in the world. We have recognized that the 3-D technique can be successfully applied and can produce a more realistic resistivity model. However, the 3-D models that we have obtained still have some ambiguities as described above. In this respect, further improvement is necessary in the 3-D inversion technology.

Acknowledgments: The authors are grateful to Yutaka Sasaki, Kyushu University, for providing 3-D MT inversion code for this work, and NEDO for giving us permission to use CSAMT field data in Bajawa. TU and TJL used a computer system at the Tsukuba Advanced Computer Center, AIST, for the computation of the 2-D and 3-D inversions.

References

Andan, A., Suhanto, E., Sukirman, A., Ashari and Usmawardi (1997) *Report on integrated geophysical investigation of Mataloko geothermal area, Ngada 2nd Regency, Nusa Tenggara Timur Province* (in Indonesian, translated to English). Volcanological Survey of Indonesia.

Arnason, K. and Flovenz, O. G. (1992) Evaluation of physical methods in geothermal exploration of rifted volcanic crust. *Geothermal Resources Council Transactions*, **16**, 207-214.

Arnason, K., Karldottir, R., Eysteinsson, H., Flovenz, O. G. and Gudlaugsson, S. T. (2000) The resistivity structure of high-temperature geothermal systems in Iceland. *Proc. World Geothermal Congress 2000*, 923-928.

Bromley, C., Khosrow, K. and Talebi, B. (2000) Geophysical exploration of Sabalan geothermal prospects in Iran. *Proc. World Geothermal Congress 2000*, 1009-1014.

deGroot-Hedlin, C. and Constable, S. (1990) Occam's inversion to generate smooth two-dimensional models from magnetotelluric data. *Geophysics*, **55**, 1613-1624.

Hursin, G. and Zhdanov M. S. (2001) Rapid 3-D magnetotelluric and CSAMT data. *Expanded Abstracts, Society of Exploration Geophysicists 71st Annual Meeting*, 1493-1498.

Johnston, J. M., Pellerin, L. and Hohmann, G. W. (1992) Evaluation of electromagnetic methods for geothermal reservoir detection. *Geothermal Resources Council Transactions*, **16**, 241-245.

Los Banos, C. E. F. (1997) 1-D interpretation of magnetotelluric data from southern Leyte geothermal project, Philippines. *United Nations University, Geothermal Training Programme Reports 1997*, 255-273.

Mackie, R., Rodi, W. and Watts, M. D. (2001) 3-D magnetotelluric inversion for resource exploration. *Expanded Abstracts, Society of Exploration Geophysicists 71st Annual Meeting*, 1501-1504.

Muraoka, H., Nasution, A., Urai, M., Takahashi, M. and Takashima, I. (2000) Regional geothermal geology of the Ngada District, central Flores, Indonesia. *Proc. World Geothermal Congress 2000,* 1473-1478.

Newman, G. and Alumbaugh, D. (2000) Three-dimensional magnetotelluric inversion using non-linear conjugate gradients. *Geophysical Journal International*, **140**, 410-424.

Ogawa, Y. and Uchida, T. (1996) A two-dimensional magnetotelluric inversion assuming Gaussian static shift. *Geophysical Journal International,* **126**, 69-76.

Rodi, W. and Mackie, R. (2001) Nonlinear

conjugate gradients algorithm for 2-D magnetotelluric inversion. *Geophysics*, **66**, 174-187.

Romo, J. M., Flores, C., Vega, R., Vazquez, R., Perez-Flores M. A., Gomez-Trevino, E., Esparza, F. J., Quijano, J. E. and Garcia, V. H. (1997) A closely-spaced magnetotelluric study of the Ahuachapan-Chipilapa geothermal field, El Salvador. *Geothermics*, **26**, 627-656.

Sasaki, Y. (1999) 3-D inversion of electrical and electromagnetic data on PC. *Proc. Second Int. Symposium on Three-Dimensional Electromagnetics*, 128-131.

Sasaki, Y. (2001) Three-dimensional inversion of static-shifted magnetotelluric data. *Proc. 5th SEGJ International Symposium*, 185-190.

Sasaki, Y. and Uchida, T. (2001) Three-dimensional inversion of magnetotelluric data with static shifts. *Extended Abstracts, Australian Society of Exploration Geophysicists 15th Geophysical Conference,* 4 pages.

Siripunvaraporn, W. and Egbert, G. (2000) An efficient data-subspace inversion method for 2-D magnetotelluric data. *Geophysics,* **65**, 791-803.

Smith, J. T. and Booker, J. R. (1991) Rapid inversion of two- and three-dimensional magnetotelluric data. *J. Geophys. Res.,* **96-B3**, 3905-3922.

Uchida, T. (1990) Reservoir structure of the Sengan geothermal field interpreted from the resistivity data (in Japanese with English abstract). *J. Geothermal Research Society of Japan,* **12**, 1-21.

Uchida, T. (1993) Smooth 2-D inversion for magnetotelluric data based on statistical criterion ABIC. *J. Geomag. Geoelectr.*, **45**, 841-858.

Uchida, T. (1995) Resistivity structure of Sumikawa geothermal field, northeastern Japan obtained from magnetotelluric data. *Proc. World Geothermal Congress 1995,* 921-925.

Uchida, T. and Ogawa, Y. (1993) Development of Fortran code for two-dimensional magnetotelluric inversion with smoothness constraint. *Geological Survey of Japan Open-File Report*, No. 205, 115p.

Uchida, T. and Mitsuhata, Y. (1995) Two-dimensional inversion and interpretation of magnetotelluric data in the Sumikawa geothermal field, Japan (in Japanese with English abstract). *Geological Survey of Japan Report*, No. 282, 17-49.

Uchida, T. and Andan, A. (1999) Preliminary interpretation of resistivity data in the Mataloko geothermal field, central Flores, Indonesia. *1998 Interim Report, Research Cooperation Project on the Exploration of Small-scale Geothermal Resources in the Eastern Part of Indonesia, Geol. Surv. Japan*, 59-70.

Uchida, T., Ogawa, Y., Takakura, S. and Mitsuhata, Y. (2000) Geoelectrical investigation the Kakkonda geothermal field, northern Japan. *Proc. World Geothermal Congress 2000,* 1893-1898.

Uchida, T., Andan, A. and Ashari (2002) Interpretation of DC resistivity data in the Bajawa geothermal field, central Flores, Indonesia. *Bulletin of Geological Survey of Japan*, **53**, 253-263.

Ussher, G., Harvey, C., Johnstone, R. and Anderson, E. (2000) Understanding the resistivities observed in geothermal systems. *Proc. World Geothermal 2000*, 1915-1920.

WestJec and MRC (2000) *FY 1999 Report on "Joint Research on Exploration of Small-Scale Geothermal Reservoirs in Remote Islands in Eastern Indonesia"* (in Japanese), 277p.

WestJec and MRC (2001) *FY 2000 Report on "Joint Research on Exploration of Small-Scale Geothermal Reservoirs in Remote Islands in Eastern Indonesia*" (in Japanese), 182p.

Zhdanov M. S., Fang, S. and Hursin, G. (2000) Electromagnetic inversion using quasi-linear approximation. *Geophysics*, **65**, 1501-1513.

Received October 4, 2001
Accepted February 21, 2002

インドネシア東部フローレス島バジャワ地熱地域における MT 法データの 2 次元及び 3 次元解析

内田利弘・Tae Jong LEE・本田　満・ASHARI・Achmad ANDAN

要　旨

地質調査総合センター，新エネルギー・産業技術総合開発機構，インドネシア鉱物資源調査局間の共同研究の一環として，インドネシア東部に位置するフローレス島バジャワ地熱地域においてMT法による比抵抗調査を実施した．得られたデータについて 2 次元解析及び 3 次元解析を行い，地熱貯留層構造について解釈を行った．解析に用いた 3 次元インバージョン手法は，平滑化拘束つきの線形化最小二乗法に基づいており，地下の比抵抗パラメタに加え，見掛比抵抗に含まれるスタティックシフトを同時に求めることができる．2 次元及び 3 次元解析モデルを比較した結果，両者が互いに整合性がとれていること，及び，本 3 次元インバージョン解析手法を実測の MT 法データに十分適用できることを確認した．しかし，2 次元解析，3 次元解析とも不完全な要素を含んでいる．地質構造が複雑で 3 次元性の強い地域に 2 次元解析を適用すると，測線下や側方にある 3 次元的構造のため，2 次元モデルには偽像が生じることがある．逆に，本研究で用いた 3 次元解析法では，均質媒質を仮定して求めたヤコビアン行列（感度行列）をすべての反復で用いているので，コントラストの大きい構造の場合，得られるモデルの信頼性が悪くなることがある．バジャワ地熱地域の中心であるマタロコ地区における比抵抗解析結果は以下のような特徴を有している．地下浅部には薄い高比抵抗層があり，これは変質をあまり受けていない火山噴出物に相当する．しかし，地表徴候のある区域では浅部から低比抵抗を示す．その下部には，調査域全体にわたって低比抵抗層が広がっている．特に地表徴候地の下は 1　ohm-m 程度の低比抵抗層であり，その層厚は 400 - 500 m 程度である．この低比抵抗層は貯留層の帽岩になっていると解釈され，浅部坑井調査からもモンモリロナイトの分布が確認されている．低比抵抗層の下には高比抵抗基盤が広がっており，これは熱水の貯留部に相当すると解釈される．高比抵抗基盤は地表徴候地の下で最も浅く（深度は約 500 m），西方に向かって急激に深くなっている．